Highly Twisted α-Diketone-Based Thermally Activated Delayed Fluorescence Emitters and their use in Organic Light-Emitting Diodes

Abhishek Kumar Gupta,[a,b] Tomas Matulaitis,[a] David B. Cordes,[a] Alexandra M. Z. Slawin,[a] Ifor D. W. Samuel[b] and Eli Zysman-Colman*[a]*

[a]Organic Semiconductor Centre, EaStCHEM School of Chemistry, University of St Andrews, Fife, KY16 9ST, UK

[b]Organic Semiconductor Centre, SUPA. School of Physics and Astronomy, University of St Andrews, North Haugh, St Andrews, Fife, KY16 9SS, UK

Keywords: TADF, OLEDs, α-diketone, red-shift emission.

Abstract

We have designed a highly twisted small TADF emitter **PXZ-α-DK** based on an α-diketone (α-DK) as a strong acceptor and phenoxazine (PXZ) as a strong donor to obtain red-shifted emission in comparison to the equivalent α-diketone linked to 9,9-dimethyl-9,10-dihydroacridine (DMAC). The **PXZ-α-DK** shows emission at 586 nm and **DMAC-α-DK** shows emission at 548 nm in 1,3-bis(*N*-carbazolyl)benzene (mCP) host at 1.5 wt% doping of the emitter, with short-delayed lifetimes of 6.9 μs for **PXZ-α-DK** and 7.6 μs for **DMAC-α-DK**. OLEDs fabricated using these emitters show green electroluminescence at 555 nm for **DMAC-α-DK**, with a maximum external quantum efficiency, EQE_{max}, of 6.3%, and orange electroluminescence at 585 nm for **PXZ-α-DK**, with an EQE_{max} of 0.8%. We corroborate the optoelectronic properties of these emitters with DFT calculations.

Introduction

Since the seminal report of Adachi and co-workers in 2012,[1] organic light-emitting diodes (OLEDs) employing organic thermally activated delayed fluorescence (TADF) emitters have received significant attention because of the potential of these materials to supplant phosphorescent complexes as they too can efficiently harvest both singlet and triplet excitons to generate light.[2,3,4] The conventional and most popular molecular design for TADF emitters relies on a highly twisted donor–acceptor (D–A) architecture that results in a small exchange integral between weakly overlapping frontier molecular orbitals, leading to a small singlet-triplet excited state energy gap, ΔE_{ST}.[1] One important key to realizing TADF is to minimize the ΔE_{ST} so as to maximize the mixing coefficient between these two states, which provides a conduit for non-emissive triplets to be converted into emissive singlets *via* reverse intersystem crossing (RISC) through thermal activation.[1,5] Among the numerous acceptor moieties that have been employed in D-A TADF systems, carbonyl-based moieties such as benzophenone derivatives have been shown to be weak acceptors, leading to several examples of blue emitters.[6–8] Further, the presence of low-lying n–π* transitions can contribute to rapid intersystem crossing (ISC) and reverse intersystem crossing (RISC) processes.[7,9] For instance, Adachi *et al.* reported a benzophenone derivative, **Px2BP** that possesses a very small ΔE_{ST} of 0.03 eV in 6 wt% doped film in 1,3-bis(*N*-carbazolyl)benzene (mCP) with a photoluminescence quantum yield, Φ_{PL}, of 70% at λ_{PL} = 538 nm leading to efficient RISC (k_{RISC} = 1×10^5 s^{-1}).[6] More recently, Wu *et al.* reported TADF

emitters containing β-diketone acceptors attached to either phenoxazine (PXZ) or 9,9-dimethyl-9,10-dihydroacridine (DMAC) as the donor moieties (**PXZPDO, PXZDMePDO**, **DMACPDO** and **DMACDMePDO**).[10] The reported Φ_{PL}, ΔE_{ST}, and delayed lifetime (τ_d) of all emitters doped in 4,4′-bis(*N*-carbazolyl)-1,1′-biphenyl (CBP) are 68%, 0.04 eV and 1.3 μs, respectively, at λ_{PL} 552 nm for **PXZPDO**; 54%, 0.07 eV, and 1.5 μs, respectively, at λ_{PL} 524 nm for **PXZMePDO**; 86%, 0.11 eV, and 1.9 μs, respectively, at λ_{PL} 524 nm for **DMACPDO**; and 64%, 0.16 eV and 1.8 μs, respectively, at λ_{PL} 497 nm for **DMACMePDO**; respectively. They also claimed **PXZPDO** and **DMACPDO** act as excited state intramolecular proton transfer (ESIPT)-based TADF molecules.[10] The OLEDs employing **PXZPDO** and **DMACPDO** achieved EQE_{max} of 18.8% and 23.3%, respectively, in vacuum-deposited devices. Our group reported TADF emitters containing β-triketone (**TPXZBM**) and β-tetraketone (**BPXZBM**) acceptors and compared their performance to **PXZPDO**.[11] All three emitters showed short τ_d of 1.3 μs for **PXZPDO**, 1.4 μs for **TPXZBM** and 1.0 μs for **BPXZBM**, due to their very small ΔE_{ST} of 0.04 eV, 0.02 eV and 0.005 eV, respectively, as 1 wt% doped films in CBP as the host matrix. Indeed, we observed that ΔE_{ST} decreases with increasing number of carbonyl groups. Notably, we demonstrated that **TPXZBM** also exhibits ESIPT. The solution-processed OLED devices with **PZXPDO**, **TPXZBM** and **BPXZBM** showed EQE_{max} values of 20.1%, 12.7% and 7.0%, respectively. [11]

In the present study, we turned our focus to the design of TADF emitters bearing a diphenyl-α-diketone (benzil) acceptor core. Benzil itself adopts a skew conformation in the ground state [O-C-C-O torsion angle of 109° and 115°, dihedral angle between phenyl groups 82° and 77°, for low temperature (< 83.5 K) and high temperature phases, respectively],[12] in reasonable agreement with the gas-phase structure calculated by DFT (O-C-C-O torsion is 126°).[13] The calculations predict that the geometry of benzil in its singlet excited state changes from the skew form to a *trans*-planar (TP) conformation (O-C-C-O torsion angle ~180°),[13] which is likely driven by a reduction of the dipolar interaction. Experimentally, upon photoexcitation at room temperature at 370 nm into the n-π* absorption band,[13] in either methylcyclohexane or ethanol, benzil shows dual emission, with a low energy unstructured band at 505 nm assigned as fluorescence from the TP conformer and a high energy structured band between 415-430 nm assigned as fluorescence from the skew conformer. However, upon excitation at 320 nm into the π-π absorption

band, another emission appears at 360 nm that is assigned to radiative decay from the S_2 state.[13] In ethanol glass at 77 K upon photoexcitation at 320 nm, emission at ca. 360 nm, assigned by the authors as originating from the S_2 state, and phosphorescence emission at 523 nm from the T_1 state were observed simultaneously. However, the emission pattern changed when the solution of benzil in ethanol was frozen while simultaneously exciting the sample at 320 nm. Under these conditions, a new emission band at 420 nm was observed, assigned as originating from the S_1 state of the skew form along with two aforesaid emissions at 360 nm and 523 nm.[13]

Unlike the β-diketone, β-triketone and β-tetraketone acceptors we previously studied, the **α-DK** acceptor is conjugated. Thus far there is just one example of a TADF compound bearing this acceptor, **DC-ACR** (renamed here as **DMAC-α-DK**).[14] Its photoluminescence maximum, λ_{PL}, at 532 nm in a 7 wt% doped film in CBP,[14] is slightly red-shifted compared to that of **DMACPDO** at 524 nm as a 6 wt% doped film in CBP,[10] indicating the stronger electron-accepting character of the α-diketone. With a goal to further red-shift the emission, we designed a new TADF emitter containing the stronger electron donor phenoxazine, **PXZ-α-DK**, (Scheme **1**). This compound showed a λ_{PL} of 586 nm compared to 548 nm for **DMAC-α-DK** as 1.5 wt% doped film in mCP and 552 nm for **PXZPDO** as 1 wt% doped film in CBP.[10] Both **DMAC-α-DK** and **PXZ-α-DK** show efficient TADF behaviour due to their effective isoenergetic singlet and triplet excited states, resulting τ_d of 7.6 and 6.9 μs, but with low Φ_{PL} of 24 and 4%. The thermally evaporated OLEDs with **DMAC-α-DK** and **PXZ-α-DK** showed EQE_{max} values of 6%, and 0.8%, respectively. Given their low Φ_{PL}, these efficiencies match the theoretical EQE_{max} values of 4.8% for **DMAC-α-DK** and 0.8% for **PXZ-α-DK**, revealing efficient triplet harvesting in these devices.

Results and discussion

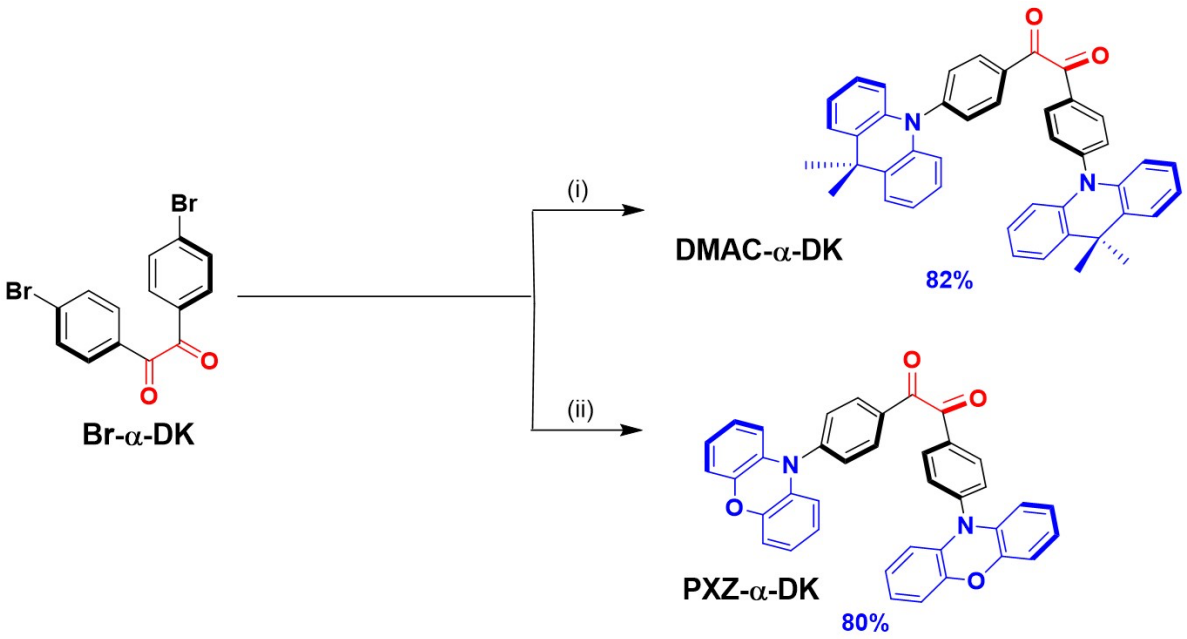

Scheme 1. Synthetic scheme. i) 9,9-dimethyl-9,10-dihydroacridine, $[Pd(OAc)_2]_3$, $[(^tBu)_3PH]BF_4$, NaO^tBu; ii) 10*H*-phenoxazine, $[Pd(OAc)_2]$, $[(^tBu)_3PH]BF_4$, NaO^tBu.

DMAC-α-DK and **PXZ-α-DK** were prepared through a palladium-catalysed Buchwald–Hartwig cross-coupling between 4,4'-dibromobenzil and DMAC or PXZ in ca. 80% yield following a previously reported procedure for the synthesis of **DMAC-α-DK** (Scheme **1**).[10] Both compounds were purified by column chromatography and further purified by temperature gradient sublimation for all studies. The identity and purity of both emitters were determined by a combination of ^1H and ^{13}C NMR spectroscopy, high-resolution mass spectrometry (HRMS), melting point determination and elemental analysis (see Experimental Section and Supporting Information Figure **S1-S8**).

Single crystals suitable for X-ray diffraction were grown by slow evaporation from a mixture of dichloromethane and hexane (**DMAC-α-DK**) or acetonitrile and hexane (**PXZ-α-DK**). The asymmetric unit of **DMAC-α-DK** contains one molecule of the emitter and one of dichloromethane solvent, while for **PXZ-α-DK** there is half a molecule of the emitter and half an acetonitrile solvent in the asymmetric unit, the symmetry-related halves of the emitter, and the symmetry-disordered solvent, are related to each other by a two-fold rotation (Figure **1**). The two carbonyl groups adopt a nearly orthogonal conformation with O-C-C-O torsion angles of 87.1(2)° and 92.9(10)° for **DMAC-α-DK** and **PXZ-α-DK**, respectively. This conformation is mirrored in the angle between the planes of the bridging phenyls, the dihedral angles being 78.2° and 77.2° for **DMAC-α-DK** and **PXZ-α-DK**, respectively. The dihedral angles between the

bridging phenylene rings and the mean plane of the central six-membered heterocycle of the donor moieties are 79.5° and 85.2° for **DMAC-α-DK**, and 79.5° for **PXZ-α-DK**. The donor groups show differing degrees of puckering; as expected from its structure, the rigid DMAC moieties in **DMAC-α-DK** show similar, moderate, degrees of puckering, with dihedral angles between the phenyl ring planes of 31.4° and 32.2°; however, the more flexible PXZ moieties in **PXZ-α-DK** are almost planar with the dihedral angle between their phenyl rings being 8.6°.

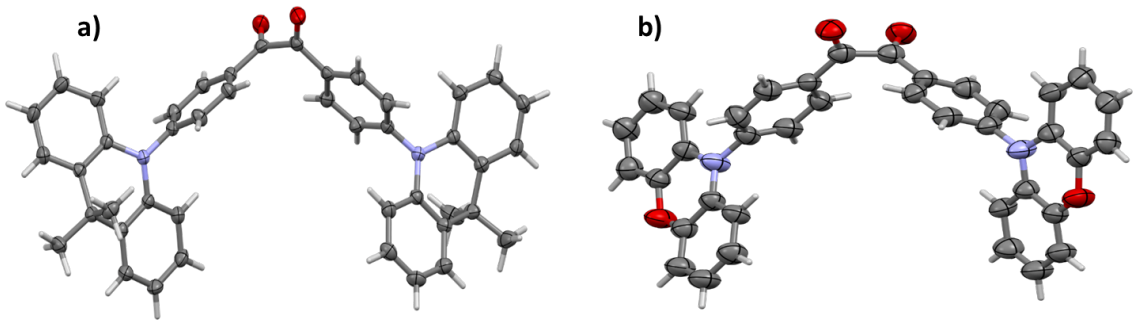

Figure 1. Thermal ellipsoid plots of the crystal structures of a) **DMAC-α-DK** and b) **PXZ-α-DK**. Ellipsoids are shown at the 50 % probability level and solvent molecules are omitted for clarity.

Both structures show a number of weak intermolecular interactions, although in different combinations. In **DMAC-α-DK** both weak hydrogen bonds and C-H···π interactions are involved, whereas in **PXZ-α-DK** the interactions are π···π as well as weak hydrogen bonds; face-to-face π-interactions being possible in this case due to the less puckered nature of the donor moiety. Three sets of C-H···π interactions are present in **DMAC-α-DK**, at H···centroid distances of 2.89-2.95 Å [C···centroid separations of 3.559(2)-3.743(2) Å], giving rise to two mutually-supporting dimers and one-dimensional chains running along the crystallographic *b*-axis. The combination of these forms a weakly-interacting three-dimensional framework which is supported by weak C-H···O hydrogen bonds between one DMAC methyl hydrogen and a ketone oxygen [H···O distance 2.70 Å, C···O separation 3.663(3) Å, C-H···O angle 168.0°] (Figure **S9**). The dichloromethane solvent is held within the framework by further C-H···O hydrogen bonds to a ketone oxygen [H···O distance 2.62 Å, C···O separation 3.402(3) Å, C-H···O angle 136.2°]. In **PXZ-α-DK** two sets of π···π interactions as well as two different C-H···O hydrogen bonds give rise to the three-dimensional structure. All the π-stacking interactions involve the aromatic rings of the PXZ moieties. One of the π-stacking interactions [centroid···centroid distance of 3.745(4)] gives rise to one-dimensional chains running along the [1 0 -1] axis. The second π-stacking interaction [centroid···centroid distance of 3.866(4)] acts in concert with one set of hydrogen bonding interactions, involving a phenyl hydrogen and the PXZ oxygen [H···O distance 2.71 Å, C···O separation 586(8) Å, C-H···O angle 153.1°] to give a one-dimensional chains along the crystallographic *c*-axis. While this π-π interaction is somewhat beyond the commonly recognized distance for such interactions, it is supported in that position by the hydrogen bonds, making it likely that both interactions contribute to forming these chains. The

second hydrogen bonding interaction, involving another phenyl hydrogen and the ketone oxygen [H···O distance 2.67 Å, C···O separation 3.292(8) Å, C-H···O angle 123.6°], gives rise to two-dimensional sheets in the (0 0 1) plane (Figure **S10**). The combination of these interactions again results in a three-dimensional framework. In a similar manner to that seen in **DMAC-α-DK**, the acetonitrile solvent is held within the framework by further C-H···O hydrogen bonds to a ketone oxygen [H···O distance 2.45 Å, C···O separation 3.30(3) Å, C-H···O angle 145.9°].

Theoretical studies

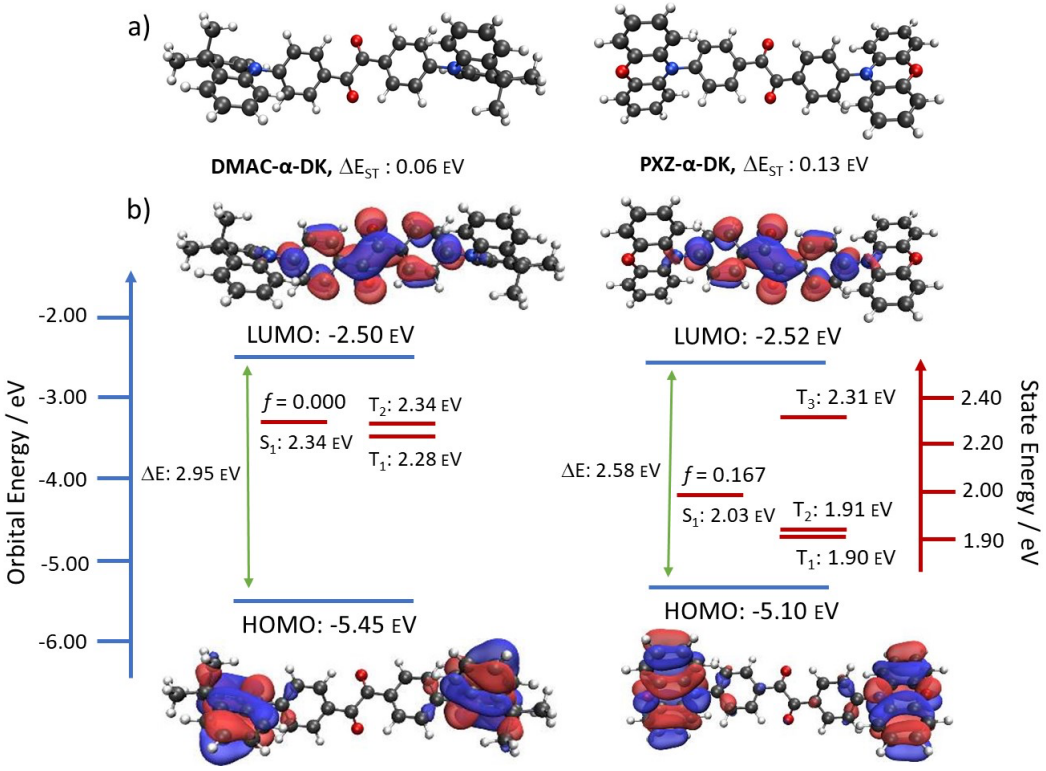

Figure 2. (a) DFT-optimized geometries of **DMAC-α-DK** and **PXZ-α-DK** and (b) their corresponding highest occupied molecular orbital (HOMO) and lowest unoccupied molecular orbital (LUMO) distributions (isovalue = 0.02), together with the transition energies for the relevant lowest singlet and triplet states calculated at the PBE0/6-31G(d,p) level in vacuum.

Density functional theory (DFT) and time-dependent DFT (TD-DFT) calculations were performed (see ESI for the computational details) to model the geometries and energies of the ground and the excited states. The ground state geometries were optimized starting from the crystal structures (Figure **2**). The DMAC units retained their puckered conformation, while the PXZ units remained planar. In **DMAC-α-DK**, the donors were found to be nearly perpendicular to the phenylene bridge (88.5°), while in **PXZ-α-DK** the PXZ moieties are less twisted (71.2°). The benzil moieties adopt a skew conformation with the α-ketone groups twisted by 129.9° and 127.2° from each other in **DMAC-α-DK** and **PXZ-α-DK**, respectively, which is different from the orthogonal arrangement found in the crystal

structure. This conformation is the same as that observed for benzil itself.[13] Both compounds exhibit a similar pattern in the distribution of the electron densities, with the HOMO localized on the donor and the LUMO localized on the benzil acceptor; there is a slight delocalization of the LUMO onto the donor moieties in **PXZ-α-DK** (Figure **2**). Due to the use of the stronger electron donor PXZ, the HOMO in **PXZ-α-DK** is destabilized at -5.10 eV compared to that in **DMAC-α-DK** at -5.45 eV. As the donor and acceptor groups show almost no conjugation, the LUMO levels of both compounds are nearly identical at -2.50 and -2.52 eV, respectively for **DMAC-α-DK** and **PXZ-α-DK**. In both compounds, there are two degenerate low-lying singlet states, each of which shows intramolecular charge transfer (ICT) character, due to the degenerate HOMO and HOMO-1 (Table **S2** and Figure **S11-S12**). The S_1 energy for **DMAC-α-DK** is 2.34 eV, while it is stabilized in **PXZ-α-DK** at 2.03 eV owing to stronger ICT, which is the result of the use of the more strongly donating PXZ donors. The T_1 state at 2.28 eV in **DMAC-α-DK** shows mainly locally excited (LE) character on the acceptor, mixed with some ICT character, and the T_2 state at 2.34 eV is ICT in nature (Figures **S2** and **S11**). The degenerate T_1 and T_2 states in **PXZ-α-DK** are purely ICT in nature while the T_3 state possesses a dominant LE character, reminiscent of the T_1 state of **DMAC-α-DK** (Table **S2**, Figure **S13**).

As the DFT optimized conformation differed from that found in the crystal structure, we also simulated the excited state behaviour of the compounds in the orthogonal α-DK conformation found the crystal structure (Figure **S16**). As expected, the interconversion barrier between orthogonal and skew conformations is very small (<15 kJ/mol and <45 kJ/mol for **DMAC-α-DK** and **PXZ-α-DK**, respectively), meaning that both conformers are accessible at room temperature. TD-DFT calculations reveal that the orthogonal conformer observed in the crystal structure of both molecules possesses a larger HOMO-LUMO gap (3.46 eV and 2.97 eV for **DMAC-α-DK** and **PXZ-α-DK**, respectively) compared to that of the respective DFT-optimized skew conformer (2.96 eV and 2.57 eV for **DMAC-α-DK** and **PXZ-α-DK**, respectively). The S_1 and T_1 energies of the orthogonal conformer are likewise destabilized for both compounds. In orthogonal **DMAC-α-DK** both states are destabilised by about 0.35 eV (S_1 and T_1 energies 2.70 eV and 2.66 eV, respectively), whereas for orthogonal **PXZ-α-DK** the extent of destabilisation is different for S_1 and T_1, at 0.28 and 0.37 eV (S_1 and T_1 energies 2.31 eV and 2.27 eV, respectively).

Electrochemistry

Cyclic voltammetry (CV) and differential pulse voltammetry (DPV) measurements were used to infer the HOMO/LUMO levels of **DMAC-α-DK** and **PXZ-α-DK** from the redox potentials. The resulting voltammograms are shown in Figure **S17** and the data are summarized in Table **1**. **DMAC-α-DK** possesses a quasi-reversible oxidation with E_{ox} at 1.04 V vs SCE, which is assigned to the oxidation of the DMAC donor moieties; this value aligns well with the previously reported E_{ox} of 1.01 V.[14] The E_{ox} of **PXZ-α-DK** is 0.83 V vs SCE, which is shifted cathodically compared to that of **DMAC-α-DK**, and is attributed to the oxidation of the **PXZ** donor moieties. The E_{ox} of **PXZ-α-DK** is similar to that of PXZPDO (E_{ox} = 0.79 V),[11] with the oxidation processes in both compounds being reversible. The estimated HOMO levels are -5.38 eV and -5.17 eV for **DMAC-α-DK** and **PXZ-α-DK**, respectively, which are in line with the values and trends calculated from DFT-optimized skew conformer (*vide supra*). The reduction waves assigned to the reduction of the benzil acceptor are quasi-reversible, at around -1.03 V vs SCE for both emitters. The corresponding LUMO energy levels for both emitters are very similar, at -3.31 V and -3.32 V for **DMAC-α-DK** and **PXZ-α-DK**, respectively. Consequently, the HOMO-LUMO energy gap of **DMAC-α-DK** (2.07 eV) is larger than that of **PXZ-α-DK** (1.85 eV).

Table 1. Electrochemical data, HOMO-LUMO levels and ΔE_{ST} values for **DMAC-α-DK** and **PXZ-α-DK**.

Emitters	E_{ox}[a] / V	E_{red}[a] / V	HOMO[b] / eV	LUMO[b] / eV	E_S/E_T[c] / eV	ΔE_{ST}[d] / eV
DMAC-α-DK	1.04	–1.03	–5.38	–3.31	2.49/2.50	0.00
PXZ-α-DK	0.83	–1.02	–5.17	–3.32	2.39/2.43	-0.04

[a] E_{ox} and E_{red} are anodic and cathodic peak potentials, respectively, obtained from DPV using F_c/F_c^+ as the internal reference and referenced versus SCE (0.46 V vs. SCE) in DCM with 0.1 M [nBu$_4$N]PF$_6$ as the supporting electrolyte.[15] [b] $E_{HOMO/LUMO} = -(E^{ox}/E^{red} + 4.8)eV$,[16] where E^{ox} is anodic peak potential and E^{red} is cathodic peak potential calculated from DPV relative to F_c/F_c^+. [c] Obtained from the onset of the prompt fluorescence (time window: 1 ns – 100 ns) and phosphorescence spectra (time window: 1 ms – 8.5 ms) of 1.5 wt% samples doped in mCP at 77 K. [d] $\Delta E_{ST} = E_S - E_T$.

Table 2. Photophysical properties of **DMAC-α-DK** and **PXZ-α-DK**

Emitters	λ_{abs} / nm (ε/ ×10^3 M^{-1}cm^{-1})	λ_{PL} / nm	τ_p / ns	τ_d / μ	Φ_{PL} / %[d]
		toluene[a]			
DMAC-α-DK	283, 366 (4.7), 410 (2.1)	410, 432, 520, 700	22.4 (51%)	1.8 (49%)	-[e]
PXZ-α-DK	283, 324 (12.1), 450 (3.2)	410, 432, 534	23.6 (49%)	1.0 (51%)	-[e]
		1.5 wt% doped in PMMA[b]			
DMAC-α-DK	277, 368, 410	536	7.6[c]	11.4[c]	10 (6)
PXZ-α-DK	270, 320, 440	410, 432, 584	7.7[c]	5.4[c]	3 (2)
		1.5 wt% doped in mCP[b,c]			
DMAC-α-DK	296, 338, 342, 372	548	9.1[c]	7.6[c]	24 (19)
PXZ-α-DK	296, 338, 342, 450	586	10.9[c]	6.9[c]	4 (3)

[a] At 298 K, values quoted are in degassed solutions, which were prepared by three freeze-pump-thaw cycles. [b] Thin films were prepared by spin-coating 1.5 wt% doped samples in PMMA and mCP. Steady-state and time-resolved emission spectra were recorded at 298 K under an O_2-free atmosphere (λ_{exc} = 366 nm for steady-state and λ_{exc} = 379 nm for time-resolved emission). [c] Average lifetime ($\tau_{avg} = \Sigma A_i\tau_i^2 / \Sigma A_i\tau_i$, where A_i is the pre-exponential for lifetime τ_i). Prompt and delayed emission were measured by TCSPC and MCS, respectively. [d] Photoluminescence quantum yields of thin films were determined using an integrating sphere (λ_{exc} = 305 nm or 340 nm) under N_2 atmosphere at 298 K. The values in parentheses are in the presence of O_2. [e] Weak emission and so Φ_{PL} was not measured.

Solution-state photophysical studies

The photophysical properties of both molecules were studied in dilute toluene solution. The absorption bands of **PXZ-α-DK** are red-shifted compared to **DMAC-α-DK**, reflecting the smaller HOMO-LUMO energy gap in the former (Figure **3** and Table **2**); the absorption spectrum for **DMAC-α-DK** matches well with that in the literature.[14] For **DMAC-α-DK**, the stronger absorption band beyond 300 nm corresponds to locally excited (LE) π-π* transitions on both the donor and acceptor moieties. The absorption band located at 320-380 nm (ε = 4.7 × 10^3 $M^{-1}cm^{-1}$ at 366 nm) is of mixed character. TD-DFT calculations assign this band to transitions to S_8 and S_{13} states that possess dominant π-π* character within the acceptor mixed with intramolecular-charge transfer transitions (ICT) from DMAC to the α-diketone, (for simulated absorption spectra, see Figure **S14a**). The weak absorption band between 380–500 nm can be attributed to the ICT transitions. TD-DFT calculations assign this band to a superposition of transitions to the $S_{1\text{-}5}$ excited states, all of which are ICT from DMAC to the α-diketone (Figures **S11** and **S14a**). Similarly, **PXZ-α-DK** possesses a stronger absorption band between 300–350 nm (at 324 nm, ε = 12 × 10^3 $M^{-1}cm^{-1}$), with a dominant π-π* transition of the PXZ mixed with ICT transitions from PXZ to the α-diketone (TD-DFT calculations predict this band to include transitions to $S_{6\text{-}12}$, Figure **S14b**), while the ICT absorption band is shifted bathochromically to 450 nm (ε = 3.2 × 10^3 $M^{-1}cm^{-1}$), see Figure **3**. The higher molar absorptivity value of this lowest energy band in **PXZ-α-DK** compared to that of **DMAC-α-DK** can be ascribed to the significantly higher oscillator strength of the ICT transitions within the former due to the relatively less twisted conformation adopted by this compound. For **PXZ-α-DK**, TD-DFT calculations predict a transition to the S_1 state with a remarkably large oscillator strength of 0.167, while in **DMAC-α-DK** the transition to the S_1 state is formally forbidden owing to the orthogonal conformation between the PXZ donors and the adjacent rings of the benzil acceptor (Figure **2**).

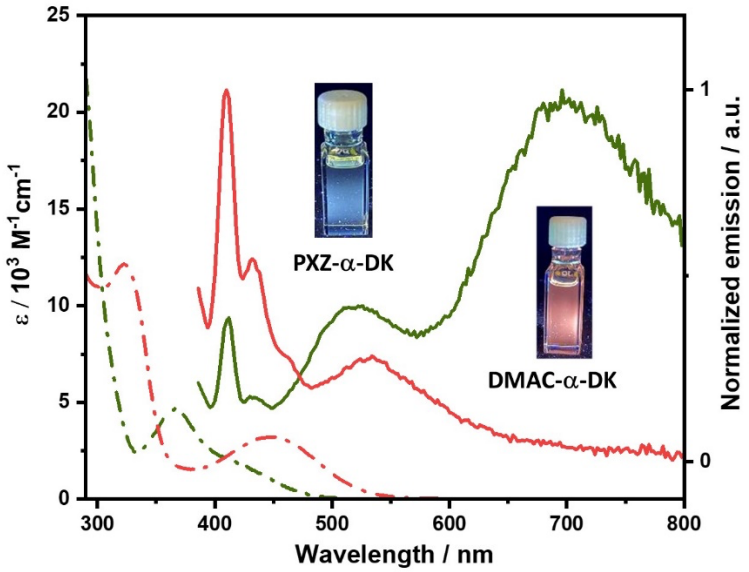

Figure 3. Molar absorptivity (dashed) and photoluminescence spectra (solid) of 5×10^{-5}M solution of **DMAC-α-DK** and 5×10^{-5}M solution of **PXZ-α-DK** in toluene at 298 K (λ_{exc} = 366 nm). Inset: Photos of photoexcited solutions in toluene.

The photoluminescence (PL) of both molecules in solution is weak, and the measured spectra in toluene are shown in Figure **3**. We find that the sharp features in the region of 410-450 nm move when the excitation wavelength is changed and therefore assign these to Raman signals from the solvent. We note that in a previous study on benzil the spectral feature located at 360 nm was attributed to the emission from S_2 state.[13] We observe a similar feature (Figure **S18**), but find it depends on excitation wavelength and therefore assign it to Raman of the solvent.

DMAC-α-DK in toluene shows two emission bands located at 520 nm and 700 nm. The weak and unstructured emission at 520 nm is assigned to emission from an ICT state, likely of the TP conformer, based on the analysis of benzil.[13] We hypothesize that the highest intensity emission located at 700 nm originates from an aggregate.[17] Aggregate formation in **DMAC-α-DK** has been reported previously.[14] For **PXZ-α-DK** we attribute the emission band at 534 nm to emission from an ICT state of the TP conformer, assigned again by analogy to the TP conformer of benzil.[13] Emission properties of **DMAC-α-DK** were previously measured in hexane,[14] therefore to qualitatively cross-compare to the data in the literature, we also conducted an additional set of measurements for **DMAC-α-DK** in hexane, exciting the sample at 335 nm and observing emission peaking at 583 nm (Figure **S19**). We again attribute

this emission to the ICT transition of the TP conformer, which is very close to the previously reported λ_{PL} at 584 nm in hexane (Figure **S19**).[14] For **PXZ-α-DK** in hexane, the main emission peak is at 650 nm (Figure **S19**).

We measured the PL decays of both molecules in toluene under degassed conditions using time-correlated single photon counting (TCSPC, Figure **4**). The ICT band in both molecules (520 nm for **DMAC-α-DK** and at 534 nm for **PXZ-α-DK**) decays with biexponential kinetics, with prompt decay lifetimes, τ_p, of 22.4 ns for **DMAC-α-DK** and 23.6 ns for **PXZ-α-DK**, and delayed lifetimes, τ_d, of 1.8 µs for **DMAC-α-DK** and, 1.0 µs for **PXZ-α-DK** (Figure **4**); the delayed emission in both cases being strongly quenched in the presence of oxygen (Figures **4**, **S20**). The time-resolved PL of **DMAC-α-DK** at 700 nm shows mono-exponential decay kinetics (τ_{PL} = 62 ns) (Figure **S21**) and is not quenched by oxygen. Further, the PL around 400 nm for both molecules is not quenched by oxygen, indicating that triplet states are not associated with this emission (Figure **S20**).

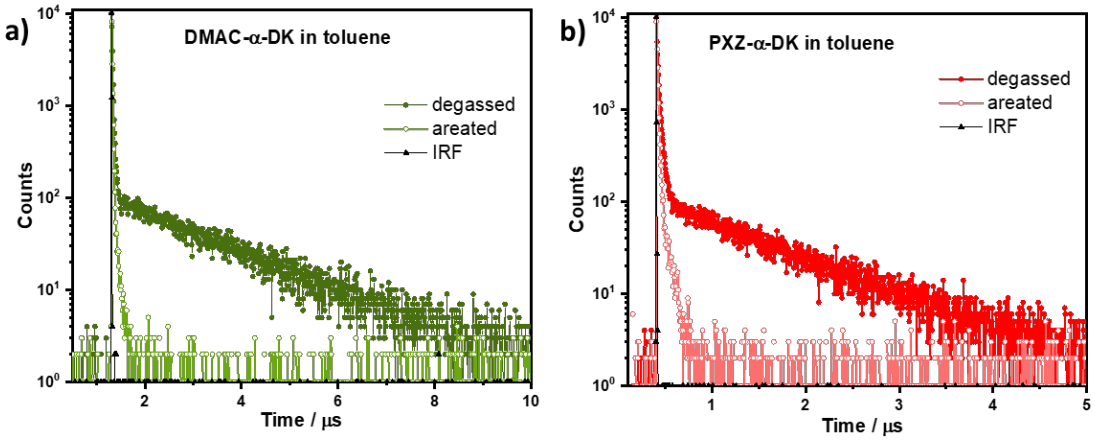

Figure 4. Time-resolved decays of a) 5×10^{-5} M **DMAC-α-DK** b) 5×10^{-5} M **PXZ-α-DK** in toluene under aerated and degassed conditions (λ_{exc} = 379 nm and λ_{em} = 525 for **DMAC-α-DK** and 535 nm for **PXZ-α-DK**).

The prompt fluorescence and phosphorescence spectra of both compounds in toluene glass at 77 K were measured to determine the S_1 and T_1 levels from their respective onsets. It should be noted that compounds are rapidly frozen such that their conformations upon photoexcitation reflect those in the ground state. The prompt fluorescence spectra of both compounds are broad and unstructured, indicating emission from an ICT state. The S_1 level of **DMAC-α-DK** (S_1 = 2.77 eV) is higher than that of **PXZ-α-DK** (S_1 = 2.44 eV), Figure **5**. The T_1 level of **DMAC-α-DK** is 2.65 eV, which is of similar magnitude and profile to that of benzil (T_1 = 2.62 eV, Figure **S22**), indicating that T_1 state

is of locally excited (^{3}LE) character on the acceptor in its skew form.[18] The corresponding ΔE_{ST} of **DMAC-α-DK** is 0.12 eV (Figure **5a**). On the other hand, **PXZ-α-DK** showed multiple contributions to the phosphorescence spectrum in toluene glass (Figure **5b**), including vibronically structured bands at higher energy than the unstructured ICT phosphorescence of **DMAC-α-DK** and the LE phosphorescence of benzil in its skew form. To rationalize the different contributions to the emission of **PXZ-α-DK,** we measured the phosphorescence of PXZ at 77 K and identified that the emission profile between 460-490 nm of **PXZ-α-DK** matches with the phosphorescence arising from PXZ. We hypothesize that the most blue-shifted contribution to the phosphorescence of **PXZ-α-DK** between 380 nm–450 nm must originate from the least conjugated conformers of **PXZ-α-DK**. These may include orthogonal conformations about the α-DK acceptor and/or conformations where the PXZ adopts a significantly more puckered geometry. Further, the unstructured emission band above 500 nm of **PXZ-α-DK** resembles that of the ICT prompt fluorescence; however, it is blue-shifted. We ascribe this blue-shift to the emission from phosphorescence resulting from the less conjugated skew conformer while the observed prompt fluorescence originates from the ICT state from the more conjugated TP conformer. Given that the observed prompt fluorescence and ICT phosphorescence of **PXZ-α-DK** in toluene glass occur from different conformers, the optically determined ΔE_{ST} value, which is less than zero, is not relevant in this case as the emitting singlet and triplet species are effectively different.

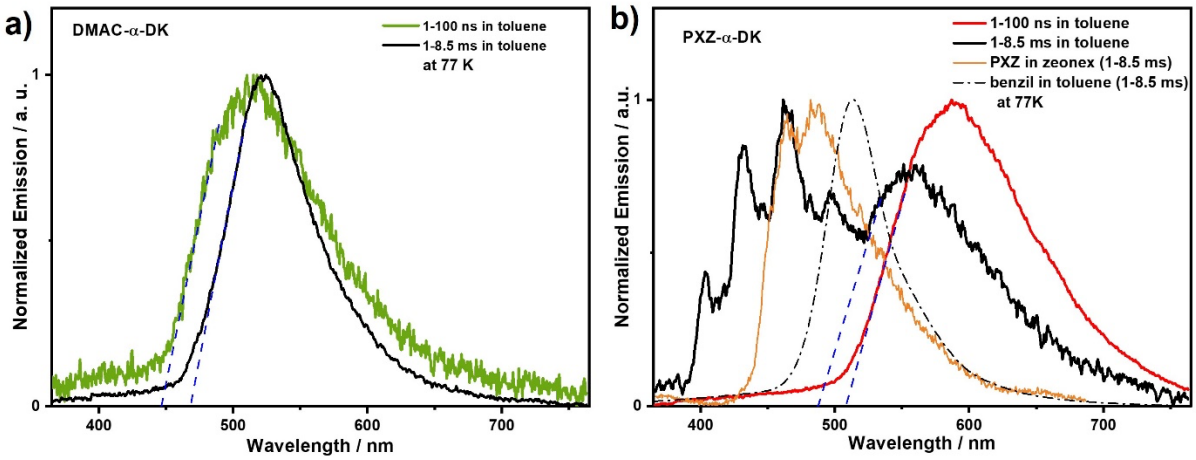

Figure 5. Prompt PL and phosphorescence spectra measurements at 77 K in toluene glass for a) **DMAC-α-DK** and b) **PXZ-α-DK** and benzil and PXZ (PXZ in zeonex). λ_{exc} = 343 nm.

Photophysical studies in thin films

We next focused our attention on the photophysical properties of **DMAC-α-DK** and **PXZ-α-DK** in doped thin films. Initially, we optimised the Φ_{PL} in poly(methylmethacrylate) (PMMA) film as the polarity of this host closely mimics that of toluene (Table **S3**). Both molecules show the highest Φ_{PL} as 1.5 wt% doped PMMA films (Table **S3**), where **DMAC-α-DK** has a Φ_{PL} of 10% and **PXZ-α-DK** has a Φ_{PL} of 3%, both under N_2 atmosphere (Table **2**). Based on the optimised Φ_{PL}, the remaining photophysical measurements were conducted on spin-coated 1.5 wt% PMMA doped films. The absorption bands of both emitters are of similar energy to those in toluene, with the weak ICT band observed in the range of 380–500 nm for **DMAC-α-DK** and at 450 nm for **PXZ-α-DK** (Figure **S23**). Upon photoexcitation at 340 nm, **DMAC-α-DK** shows unstructured ICT-based emission at 536 nm, which is 574 cm^{-1} (16 nm) red-shifted compared to the λ_{PL} in toluene, while the ICT-based emission for **PXZ-α-DK** at 584 nm is 1603 cm^{-1} (50 nm) red-shifted (Figure **S24**). We also observed weak LE emission between 400–450 nm for **PXZ-α-DK** (Figure **S24**), similar to that measured in toluene. On increasing the doping concentration to 10 wt% in PMMA, the Φ_{PL} decreased and the λ_{PL} red-shifted to 566 nm (Φ_{PL} = 2.7%) for **DMAC-α-DK** and 604 nm (Φ_{PL} = 1.4%) for **PXZ-α-DK** (Figure **S24**), likely due to increased contribution from aggregates.[17] As shown in **Error! Reference source not found.25**, the 1.5 wt% doped films showed multiexponential decay kinetics with average $\tau_{p,}$ of 7.6 ns and 7.7 ns and average τ_d of 11.4 µs and 5.4 µs for **DMAC-α-DK** and **PXZ-α-DK**, respectively. The average prompt lifetime is quite similar for both molecules; however, the delayed lifetime in **DMAC-α-DK** is much longer than that in **PXZ-α-DK**.

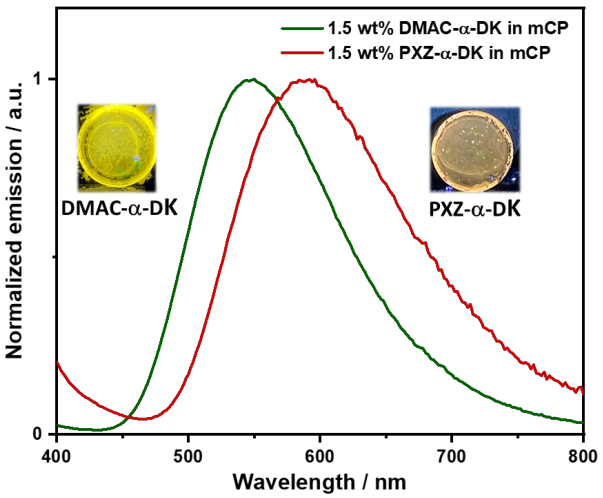

Figure 6. Photoluminescence spectra of **DMAC-α-DK** and **PXZ-α-DK** dispersed at 1.5 wt% in mCP matrix at 295 K (λ_{exc} = 340 nm). Inset: Photos of photoexcited thin films.

We then investigated the photophysical behaviour of both emitters in an OLED-relevant host, mCP, that has a suitably high triplet energy of 2.91 eV.[19] A concentration study of both emitters revealed that the Φ_{PL} is highest in 1.5 wt% doped films in mCP (Table **S3**), at 24% for **DMAC-α-DK** and 4% for **PXZ-α-DK**. It should be noted that the reported Φ_{PL} of a 7 wt% doped film of **DMAC-α-DK** in CBP is 13%.[14] Both the absorption and emission spectra for **DMAC-α-DK** and **PXZ-α-DK** are very similar to those measured in PMMA (Figure **6** and Figure **S26**). The temperature-dependent time-resolved PL decays in mCP are shown in Figure **7**. The time-resolved PL decays in mCP show a nanosecond prompt emission and a delayed emission with a microsecond delayed lifetime (Table **2**), with values comparable to those measured in PMMA. The average τ_d of 1.5 wt% **DMAC-α-DK** in mCP is 7.6 µs while that for the 1.5 wt% **PXZ-α-DK** doped in mCP is 6.9 µs. The prompt emission is insensitive to temperature while the delayed emission is thermally activated, a behaviour consistent with TADF.

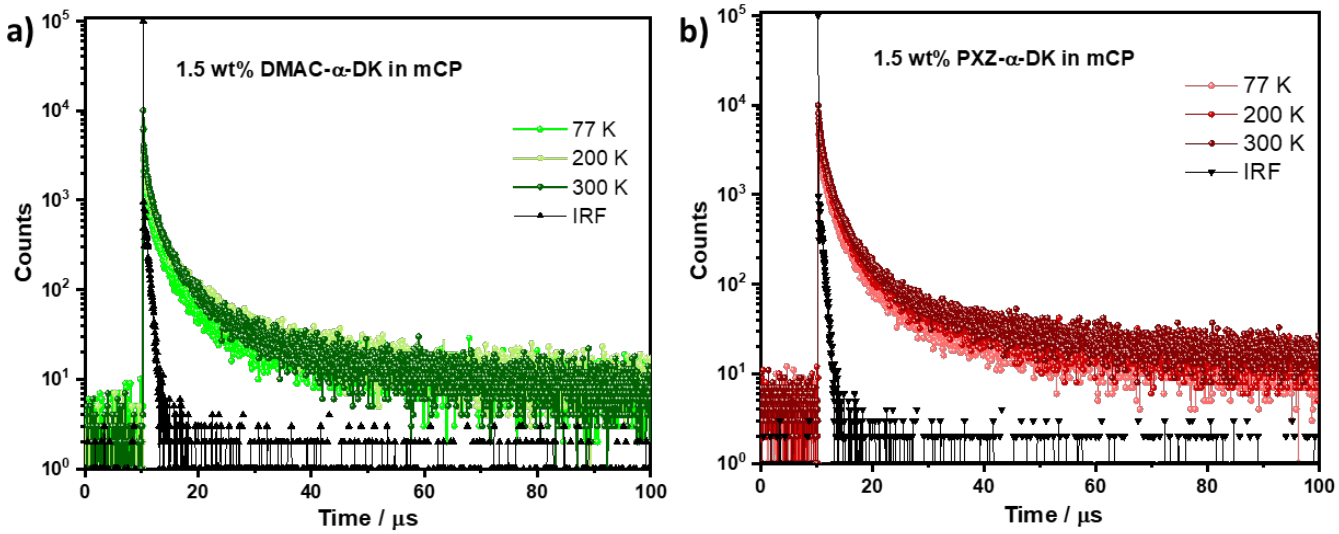

Figure 7. Temperature-dependent PL decays by TCSPC of 1.5 wt% mCP doped films of (a) **DMAC-α-DK** and (b) **PXZ-α-DK**. IRF is the instrument response function (λ_{exc} = 379 nm and λ_{em} = 550 nm for **DMAC-α-DK** and 590 nm for **PXZ-α-DK**).

We next measured the prompt fluorescence and phosphorescence spectra of the doped films in both PMMA and mCP at 77 K to determine the S_1 and T_1 levels from their respective onsets (Figure **8** and **S27**). We found broad and

unstructured prompt fluorescence for both compounds in both PMMA and mCP, indicating emission from an ICT state. The S_1 levels in 1.5 wt% doped PMMA films were found to be 2.69 eV and 2.51 eV for **DMAC-α-DK** and **PXZ-α-DK**, respectively (Figure **S27**). The S_1 levels of both emitters in mCP are stabilized compared to those in 1.5 wt% doped PMMA films at 2.50 eV and 2.39 eV for **DMAC-α-DK** and **PXZ-α-DK**, respectively.

The shape and spectral position of the **DMAC-α-DK** phosphorescence in both PMMA and mCP resemble that of benzil (Figures **8**, **S22**, **S27**). The corresponding T_1 levels of **DMAC-α-DK** are 2.56 eV in PMMA, and 2.50 eV in mCP. Subsequently, ΔE_{ST} of **DMAC-α-DK** is 0.12 eV in PMMA (Figure **S27**), and effectively 0 eV in mCP (Figure **8**); the reported ΔE_{ST} of the 7 wt% **DMAC-α-DK** doped film in CBP is 0.01 eV.[14]

The **PXZ-α-DK** phosphorescence in PMMA and mCP is broad and unstructured (Figures **8**, **S27**). However, in both PMMA and mCP there is a clear blue-shift of the phosphorescence compared to the prompt emission. The T_1 energy of **PXZ-α-DK** in PMMA (2.55 eV) is very close to that of **DMAC-α-DK** in PMMA, suggesting that in PMMA there is a significant contribution from the LE states within the acceptor to the overall **PXZ-α-DK** phosphorescence. The shape of the **PXZ-α-DK** phosphorescence in mCP resembles that of prompt emission, and in addition, the blue edge onset is the same for both prompt and phosphorescence emission. This indicates that the emission originates from ICT states; however, the phosphorescence spectrum is blue-shifted compared to the prompt fluorescence. The corresponding apparent ΔE_{ST} values of **PXZ-α-DK** are -0.04 eV in both PMMA and mCP. A plausible explanation for this apparent inverted singlet-triplet gap is that the blue-shifted phosphorescence results from emission from the skew conformer, with the decay of the phosphorescence of the trans planar conformer already largely complete while the prompt fluorescence is dominated by the TP conformer.

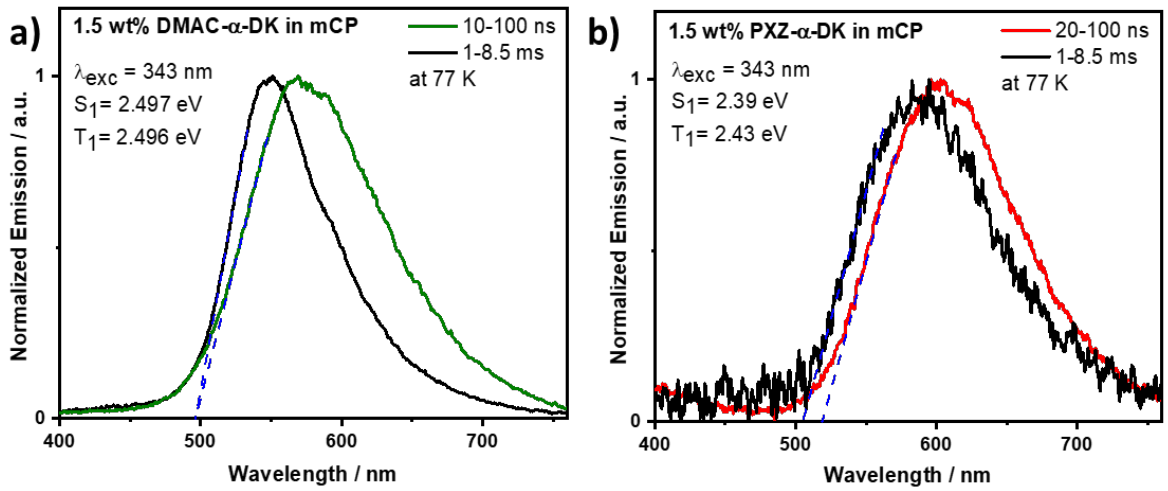

Figure 8. 77 K prompt PL and phosphorescence spectra measurement of 1.5 wt% a) **DMAC-α-DK** and (b) **PXZ-α-DK** doped in mCP host (λ_{exc} = 343 nm), the ΔE_{ST} value is taken from the onset value difference between the 77 K prompt fluorescence and phosphorescence spectra.

OLEDs characterization

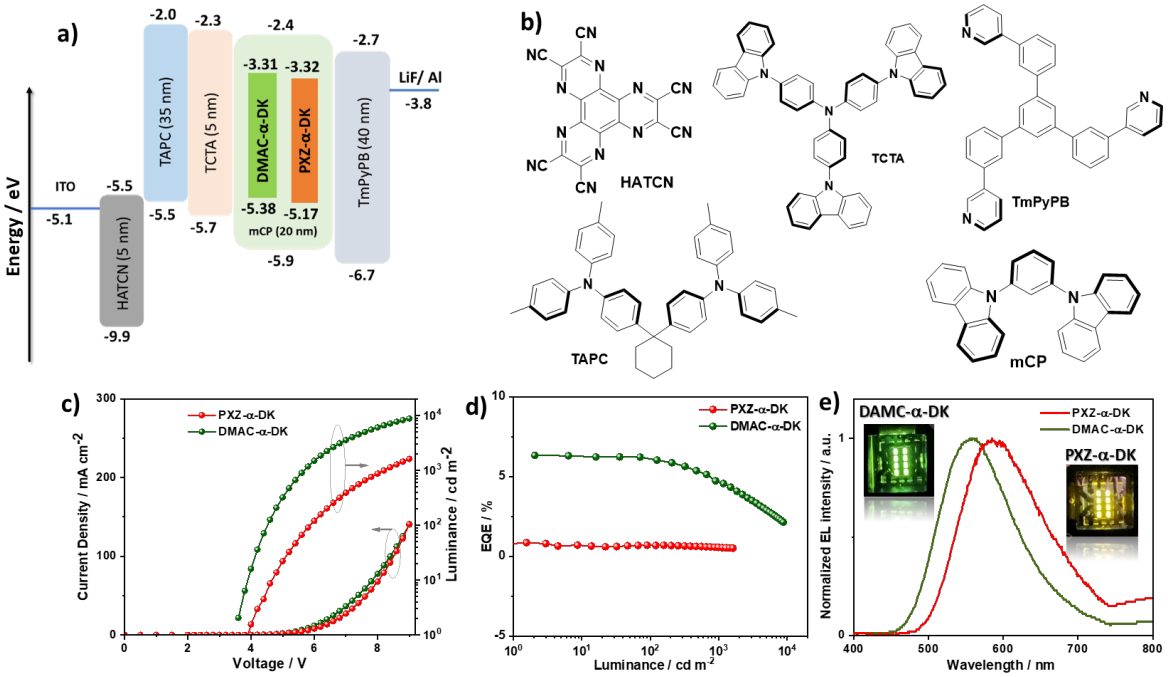

Figure 9. (a) Energy level diagram of materials employed in the devices; (b) Molecular structure of materials used in the devices; (c) Current density and luminescence versus voltage characteristics for the devices; (d) External quantum efficiency versus luminescence curves for the devices; (e) Electroluminescence spectra of the device of **DMAC-α-DK** and **PXZ-α-DK**. Inset: photos of the devices.

OLED devices based on **PXZ-α-DK** and **DMAC-α-DK** were fabricated by vacuum deposition using a typical bottom-emitting OLED device architecture (Figure **9a**) that consists of indium tin oxide (ITO)/ 1,4,5,8,9,11-hexaazatriphenylenehexacarbonitrile (HATCN) (5 nm)/ 1,1-bis[(di-4-tolylamino)phenyl]cyclohexane (TAPC) (35

347 nm)/tris(4-carbazoyl-9-ylphenyl)amine (TCTA) (5 nm)/emissive layer (20 nm)/1,3,5-tri[(3-pyridyl)-phen-3-
348 yl]benzene (TmPyPB) (65 nm)/LiF (0.6 nm)/Al (100 nm), where HATCN, TAPC and TCTA play the roles of hole
349 injection layer (HIL), hole transportation layer (HTL) and electron blocking layer (EBL), respectively. The TmPyPB
350 acts both as an electron transport layer (ETL) and a hole blocking layer due to its deep HOMO (-6.7 eV),[20] and LiF
351 acts as an electron injection layer (EIL). The molecular structures of the materials used in these OLEDs are shown in
352 Figure **9b**. The emission layer (EML) is composed of 1.5 wt% of either **PXZ-α-DK** or **DMAC-α-DK** doped into mCP,
353 based on the Φ_{PL}-doping study (Table **S3**). The performance of the OLEDs is summarized in EQEmax **of** both emitters
354 is very close to the theoretically calculated EQEmax of 4.8% for **DMAC-α-DK** and 0.8% for **PXZ-α-DK**, when
355 considering an outcoupling efficiency of χout ≈ 20%**.**

356 **Table** ***1***. Current density–voltage–brightness (J–V–L) curves, EQE–luminance curves and electroluminescence
357 spectra (EL) are shown in **Error! Reference source not found.9**. As shown in Figure **9e,** the EL spectra of the OLEDs
358 are similar to the corresponding PL spectra of the emitters in the thin film, with EL maxima, λ_{EL}, at 555 nm for **DMAC-**
359 **α-DK** and 585 nm for **PXZ-α-DK**. The corresponding CIE coordinates are (0.420, 0.531) and (0.506, 0.481) for the
360 devices with **DMAC-α-DK** and **PXZ-α-DK**, respectively. The turn-on voltage of devices based on **DMAC-α-DK** and
361 **PXZ-α-DK** are 3.6 V and 3.9 V, respectively, and is dependent on the energy gap between the HOMO of materials
362 used in the HTL and EML layers. The device based on **DMAC-α-DK** showed a maximum external quantum efficiency,
363 EQE_{max}, of 6.3%, a maximum current efficiency (CE_{max}) of 18.36 cd/A and maximum power efficiency (PE_{max}) of 16.45
364 lm/W (EQEmax **of** both emitters is very close to the theoretically calculated EQEmax of 4.8% for **DMAC-α-DK** and
365 0.8% for **PXZ-α-DK**, when considering an outcoupling efficiency of χout ≈ 20%**.**

366 **Table** ***1*** and Figures **S28** and **S29**); this efficiency is comparable to that of the literature-reported device with the
367 same emitter, but where the EML consisted of 1 wt% **DMAC-α-DK** in CBP.[14] The EQE_{max} of the device based on **PXZ-**
368 **α-DK** is 0.83%, with CE_{max} = 1.99 cd/A and PE_{max} = 1.52 lm/W. Devices of both emitters showed low efficiency roll-
369 off at high luminance, with an EQE of 6.14% at 100 cd/m^2 and 4.73% at 1,000 cd/m^2 for the **DMAC-α-DK-**based
370 device and an EQE of 0.73% at 100 cd/m^2 0.62% at 1,000 cd/m^2 for **PXZ-α-DK**. The maximum brightness of the OLED
371 containing **DMAC-α-DK** reached 8,817 cd/m^2 at an EQE of 2.14%, while the OLED containing **PXZ-α-DK** reached

1,617 cd/m^2 at an EQE of 0.51%. The EQE_{max} of both emitters is very close to the theoretically calculated EQE_{max} of 4.8% for **DMAC-α-DK** and 0.8% for **PXZ-α-DK**, when considering an outcoupling efficiency of $\chi_{out} \approx 20\%$.

Table 1. Electroluminescence data for the devices.

Emitter	Host	V_{on}[a] / V	λ_{EL}[b] / nm	CE[c] / cd A^{-1}	PE_{max} / lm W^{-1}	EQE[c] / %	CIE[d] / x,y
DMAC-α-DK	mCP (1.5%)	3.6	555	18.36	16.45	6.33/6.14/4.73	0.420, 0.531
PXZ-α-DK	mCP (1.5%)	3.9	585	1.92	1.55	0.83/0.73/0.62	0.506, 0.481

[a] The turn-on voltage at a brightness 1 cd m^{-2}. [b] The electroluminescence maximum recorded at 5 V. [c] EQE_{max}/EQE_{100}/ EQE_{1000}. [d] The CIE coordinates recorded at 6 V.

Conclusions

Here we presented a cross-comparison of the optoelectronic and OLED device properties of two TADF donor-acceptor compounds bearing an α-diketone acceptor moiety. The use of the stronger phenoxazine donor in **PXZ-α-DK** red-shifted the emission to 586 nm compared to **DMAC-α-DK** at 548 nm in 1.5 wt% mCP doped films. **PXZ-α-DK** shows complex emission behaviour in toluene glass. The presence of a highly twisted conformation in these two compounds resulted in essentially isoenergetic S_1 and T_1 states, short-delayed lifetimes and low photoluminescence quantum yields. Green and orange OLEDs were fabricated showing an EQE_{max} of 6.3% for the **DMAC-α-DK** based device at λ_{EL} = 555 nm with CIE coordinates of (0.420, 0.531) and 0.8% for **PXZ-α-DK** at λ_{EL} = 585 nm with CIE coordinates of (0.506, 0.481).

Acknowledgment

AKG is grateful to the Royal Society for Newton International Fellowship NF171163. We acknowledge support from the Engineering and Physical Sciences Research Council of the UK (grants EP/P010482/1 and EP/L017008/1). We are also grateful for financial support from the University of St Andrews Restarting Research and Restarting Interdisciplinary Research Funding Schemes (SARRF and SARIRF) which are funded through the Scottish Funding Council grant reference SFC/AN/08/020.

Supporting Information

The following files are available free of charge. Compound characterization (^{1}H NMR, ^{13}C NMR, elemental analysis, HRMS), SCXRD, photophysical studies, OLEDs data, DFT calculations. Crystallographic information for **DMAC-α-DK** and **PXZ-α-DK** (CCDC: 2094658, 2094659).

References

(1) Uoyama, H.; Goushi, K.; Shizu, K.; Nomura, H.; Adachi, C. Highly Efficient Organic Light-Emitting Diodes from Delayed Fluorescence. *Nature* **2012**, *492* (7428), 234–238. https://doi.org/10.1038/nature11687.

(2) Kaji, H.; Suzuki, H.; Fukushima, T.; Shizu, K.; Suzuki, K.; Kubo, S.; Komino, T.; Oiwa, H.; Suzuki, F.; Wakamiya, A.; Murata, Y.; Adachi, C. Purely Organic Electroluminescent Material Realizing 100% Conversion from Electricity to Light. *Nat. Commun.* **2015**, *6* (May), 2–9. https://doi.org/10.1038/ncomms9476.

(3) Wong, M. Y.; Zysman-Colman, E. Purely Organic Thermally Activated Delayed Fluorescence Materials for Organic Light-Emitting Diodes. *Adv. Mater.* **2017**, *29* (22), 1605444. https://doi.org/10.1002/adma.201605444.

(4) Yang, Z.; Mao, Z.; Xie, Z.; Zhang, Y.; Liu, S.; Zhao, J.; Xu, J.; Chi, Z.; Aldred, M. P. Recent Advances in Organic Thermally Activated Delayed Fluorescence Materials. *Chem. Soc. Rev.* **2017**, *46* (3), 915–1016. https://doi.org/10.1039/c6cs00368k.

(5) Zhang, Q.; Li, B.; Huang, S.; Nomura, H.; Tanaka, H.; Adachi, C. Efficient Blue Organic Light-Emitting Diodes Employing Thermally Activated Delayed Fluorescence. *Nat. Photonics* **2014**, *8* (4), 326–332. https://doi.org/10.1038/nphoton.2014.12.

(6) Lee, S. Y.; Yasuda, T.; Yang, Y. S.; Zhang, Q.; Adachi, C. Luminous Butterflies: Efficient Exciton Harvesting by Benzophenone Derivatives for Full-Color Delayed Fluorescence OLEDs. *Angew. Chemie - Int. Ed.* **2014**, *53* (25), 6402–6406. https://doi.org/10.1002/anie.201402992.

(7) Wolf, M. W.; Legg, K. D.; Brown, R. E.; Singer, L. A.; Parks, J. H. Photophysical Studies on the Benzophenones. Prompt and Delayed Fluorescences and Self-Quenching. *J. Am. Chem. Soc.* **1975**, *97* (16), 4490–4497. https://doi.org/10.1021/ja00849a008.

(8) Kreiza, G.; Banevičius, D.; Jovaišaitė, J.; Maleckaitė, K.; Gudeika, D.; Volyniuk, D.; Gražulevičius, J. V.; Juršėnas, S.; Kazlauskas, K. Suppression of Benzophenone-Induced Triplet Quenching for Enhanced TADF Performance. *J. Mater. Chem. C* **2019**, *7* (37), 11522–11531. https://doi.org/10.1039/c9tc02408e.

(9) Kearns, D. R.; Case, W. A. Phosphorescence Excitation Method . III . Aromatic Ketones and Aldehydes. **1966**, *2* (18), 5087–5097.

(10) Wu, K.; Zhang, T.; Wang, Z.; Wang, L.; Zhan, L.; Gong, S.; Zhong, C.; Lu, Z. H.; Zhang, S.; Yang, C. De Novo Design of Excited-State Intramolecular Proton Transfer Emitters via a Thermally Activated Delayed Fluorescence Channel. *J. Am. Chem. Soc.* **2018**, *140* (28), 8877–8886. https://doi.org/10.1021/jacs.8b04795.

(11) Gupta, A. K.; Li, W.; Ruseckas, A.; Lian, C.; Carpenter-Warren, C. L.; Cordes, D. B.; Slawin, A. M. Z.; Jacquemin, D.; Samuel, I. D. W.; Zysman-Colman, E. Thermally Activated Delayed Fluorescence Emitters with Intramolecular Proton Transfer for High Luminance Solution-Processed Organic Light-Emitting Diodes. *ACS Appl. Mater. Interfaces* **2021**, *13* (13), 15459–15474. https://doi.org/10.1021/acsami.1c02248.

(12) More, M.; Odou, G.; Lefebvre, J. Structure Determination of Benzil in Its Two Phases. *Acta Crystallogr. Sect. B* **1987**, *43* (4), 398–405. https://doi.org/10.1107/S0108768187097660.

(13) Bhattacharya, B.; Jana, B.; Bose, D.; Chattopadhyay, N. Multiple Emissions of Benzil at Room Temperature

and 77 K and Their Assignments from Ab Initio Quantum Chemical Calculations. *J. Chem. Phys.* **2011**, *134* (4). https://doi.org/10.1063/1.3533797.

(14) Cai, X.; Li, X.; Xie, G.; He, Z.; Gao, K.; Liu, K.; Chen, D.; Cao, Y.; Su, S.-J. "Rate-Limited Effect" of Reverse Intersystem Crossing Process: The Key for Tuning Thermally Activated Delayed Fluorescence Lifetime and Efficiency Roll-off of Organic Light Emitting Diodes. *Chem. Sci.* **2016**, *7* (7), 4264–4275. https://doi.org/10.1039/C6SC00542J.

(15) Connelly, N. G.; Geiger, W. E. Chemical Redox Agents for Organometallic Chemistry. *Chem. Rev.* **1996**, *96* (2), 877–910. https://doi.org/10.1021/cr940053x.

(16) Cardona, C. M.; Li, W.; Kaifer, A. E.; Stockdale, D.; Bazan, G. C. Electrochemical Considerations for Determining Absolute Frontier Orbital Energy Levels of Conjugated Polymers for Solar Cell Applications. *Adv. Mater.* **2011**, *23* (20), 2367–2371. https://doi.org/10.1002/adma.201004554.

(17) Woon, K. L.; Yi, C. L.; Pan, K. C.; Etherington, M. K.; Wu, C. C.; Wong, K. T.; Monkman, A. P. Intramolecular Dimerization Quenching of Delayed Emission in Asymmetric D-D'-A TADF Emitters. *J. Phys. Chem. C* **2019**, *123* (19), 12400–12410. https://doi.org/10.1021/acs.jpcc.9b01900.

(18) Roy, D. S.; Bhattacharyya, K.; Bera, S. C.; Chowdhury, M. Conformational Relaxation in the Excited Electronic States of Benzil and Naphthyl. *Chem. Phys. Lett.* **1980**, *69* (1), 134–140. https://doi.org/https://doi.org/10.1016/0009-2614(80)80030-3.

(19) Kawamura, Y.; Goushi, K.; Brooks, J.; Brown, J. J.; Sasabe, H.; Adachi, C. 100% Phosphorescence Quantum Efficiency of Ir (III) Complexes in Organic Semiconductor Films. *Appl. Phys. Lett.* **2005**, *86* (7), 1–3. https://doi.org/10.1063/1.1862777.

(20) Su, S. J.; Chiba, T.; Takeda, T.; Kido, J. Pyridine-Containing Triphenylbenzene Derivatives with High Electron Mobility for Highly Efficient Phosphorescent OLEDs. *Adv. Mater.* **2008**, *20* (11), 2125–2130. https://doi.org/10.1002/adma.200701730.

Table of content: